NANO LETTERS

2007
Vol. 7, No. 7
1856−1862

C–BN Patterned Single-Walled Nanotubes Synthesized by Laser Vaporization

Shaïma Enouz,[†,‡] Odile Stéphan,[§] Jean-Lou Cochon,[||] Christian Colliex,[§] and Annick Loiseau*,[†]

LEM, CNRS-ONERA (UMR104), 29 av. de la Division Leclerc, BP72, 92322 Châtillon Cedex, France, LCVN (UMR5581), Université de Montpellier II, 34095 Montpellier Cedex 5, France, LPS (UMR 8502), Université Paris-Sud, Bât. 510, 91405 Orsay Cedex, France, and DMSC, ONERA, Chemin de la Hunière, 91761 Palaiseau Cedex, France

Received February 9, 2007; Revised Manuscript Received May 14, 2007

ABSTRACT

We report on the synthesis of C–BN single-walled nanotubes made of BN nanodomains embedded into a graphene layer. The synthesis process consists of vaporizing, by a continuous CO_2 laser, a target made of carbon and boron mixed with a Co/Ni catalyst under N_2 atmosphere. High-resolution transmission electron microscopy (HRTEM) and nanoelectron energy loss spectroscopy (nanoEELS) provide direct evidence that boron and nitrogen co-segregate with respect to carbon and form nanodomains within the hexagonal lattice of the graphene layer in a sequential manner. A growth model is proposed to account for the observed C–BN self-organization and to explain how kinetics and local energetics at intermediate states can tailor ultimate single layer BN–C heterojunctions.

Nanotubes have attracted extensive interest in the past decade because of their unique structural and physical properties. Carbon nanotubes (CNTs) exhibit semiconducting or metallic characteristics, with a band gap close to 1 eV.[1] Boron nitride nanotubes (BNNTs) possess the same hexagonal structure, with boron and nitrogen atoms on alternate lattice sites. Experimental investigations report a wide band gap close to 6 eV, independent of the tube diameter and chirality contrary to pure carbon nanotubes, as predicted and confirmed theoretically.[2−6] Up to now, it is still difficult to control the geometrical structure of carbon nanotubes that tune the electronic properties. In this context, synthesizing nanotubes made of carbon and of chemical elements having different electronegativities with respect to carbon such as B and N (B: 2.0; C: 2.5; N: 3.1)[7] is expected to be a promising approach for tailoring the electronic properties of nanotubes as a function of their chemical composition.[8,9] Among the different possibilities, special attention has been brought to CB_xN_y nanotubes. First, the ternary BC_2N compound has been theoretically predicted to be stable with electronic properties intermediate between graphite and h-BN.[2,10] Second, energetic bonding considerations indicate that C−B (2.59 eV) and C−N (2.83 eV) bonds are less stable than C−C (3.7 eV) and B−N (4 eV) bonds.[7] Indeed, CALPHAD calculations of the B−C−N phase diagram show complete phase segregation between graphite and h-BN with no intermediate phase.[11,12] Applying these properties to tubular structures, one may expect to assemble in a nanotube device segment of structures having different electronic properties. Theoretical calculations indicate that the graphite/h-BN phase separation could lead to the formation, within a single-walled nanotube, of C−BN heterojunctions or superlattices, and even quantum dots.[7,8,13] One can in turn consider using these properties to adjust the synthesis conditions in order to produce SWNTs with anticipated BC patterning with new electronic, optical, or magnetic properties.

Synthesis of such heterostructures is therefore highly desirable. Original work on the synthesis of h-BCN structures has been performed since 1987,[14] and the study of the optical properties of such structures has been performed with a demonstration of photoluminescence in the visible range.[15,16]

Experimentally, the segregation between graphite and h-BN has been achieved in CB_xN_y nanotubes, but it has until now been restricted to multiwalled nanotubes.[17−24] The first direct synthesis was carried out in 1994 using the arc-discharge method.[17] Spatially resolved chemical analysis using EELS provided an experimental evidence that the three kinds of elements were not mixed atomically but that boron

* Corresponding author. E-mail: annick.loiseau@onera.fr.
[†] LEM, CNRS-ONERA (UMR104).
[‡] LCVN (UMR5581), Université de Montpellier II.
[§] LPS (UMR 8502), Université Paris-Sud.
[||] DMSC, ONERA.

10.1021/nl070327z CCC: $37.00
Published on Web 06/22/2007

and nitrogen formed small (typically from a few to 10 nm) domains embedded in the graphene network. Again using the arc-discharge method, an interesting geometry of coaxial nanocable with a C−BN−C sandwich structure was obtained and identified thanks to spatially resolved EELS.[25] The radial C−BN segregation was found to be a natural self-organization resulting from the phase separation between graphite and h-BN occurring during the growth.[20] Later on, various sandwich multiwalled structures were obtained using various synthesis methods and postprocessing treatments of C MWNTs.[18,19,21,22,25,26] Moreover, for electronic and photonic applications, Han et al. have achieved the aligned growth needed using both a pyrolysis and substitution reaction route.[27,28] In some cases, however, it seems that, depending on the processing conditions, a homogeneous distribution of C, B, and N within the layers can also be observed.[29−31] Concerning the synthesis of SWNTs, we can note the work of Zhi et al.[32] The authors observed the presence of CB_xN_y SWNTs on the tip of the spines on the surface of MWNTs with cactus-like structure. More recently, homogeneous B−C−N SWNTs have been produced using a hot-filament CVD process.[33]

In this letter, we show that the graphite/h-BN phase separation can be tailored within a single layer and we present a direct synthesis route to a new kind of single-walled nanotubes made of graphene and BN pieces self-organized in a sequential manner along the tube axis.

In the present study, synthesis of CB_xN_y single-walled nanotubes has been carried out using the original continuous laser vaporization reactor that we have developed at ONERA and which has already shown its efficiency for the synthesis of C SWNTs[34] and BN SWNTs.[35] We briefly recall the principle of this technique and describe the special conditions we have used for getting nanotubes made of C, B, and N. The synthesis method consists in vaporizing a target, at 3750 K, by a CO_2 continuous laser ($\lambda = 10.6\ \mu$m, 1.5 kW) and to condense the vapor under a temperature gradient created by the laminar circulation of a gas from the bottom to the top of the reactor chamber. For the synthesis of C SWNTs, the target is made of a graphite powder mixed with catalyst powders (Ni/Co, 2:2 atom %), whereas for the synthesis of BN SWNTs, it is made of a h-BN powder. In this work, we doped the targets used for C SWNTs (i.e., with a metallic catalyst) with a pure boron powder (5 atom %). The source of nitrogen was, as for the synthesis of BN SWNTs, insured by filling the reactor with a nitrogen gas under a pressure of 300 hPa and a flow rate of 50 sccm. Synthesis products were ultrasonically dispersed in absolute ethanol for 15 min and deposited on grids for transmission electron microscopy (TEM) studies and for the electron energy loss spectroscopy (EELS) experiments. A high-resolution TEM (Zeiss Libra, 200 kV) was used for studying the structure of the nanotubes and spatially resolved chemical, and bonding analyses by EELS were carried out in a dedicated STEM VG HB 501 using the spectrum-imaging mode.[36,37]

HRTEM characterization (Figure 1) shows the presence of different nanostructures in the sample: nanotubes where the relative fraction of SWNTs with respect to MWNTs is about 90% amorphous or partially graphitized materials and nanoparticles. The SWNT/MWNT ratio has been determined from statistical inspection of several zones of the soot. Most SWNTs are self-assembled in crystalline ropes. Their structural analysis has revealed a diameter distribution centered at 1.35 nm. Their length may be far longer than 1 μm. Furthermore, they are observed to be always completely empty, with no foreign nanostructure such as aggregates or inner tubes encapsulated in the hollow core.

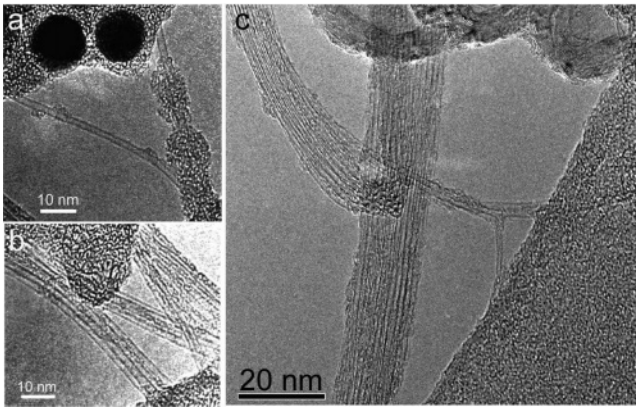

Figure 1. HRTEM images of BN-doped single-walled carbon nanotubes. Images of both isolated SWNTs and Ni + Co nanoparticles in (a) and rope of nanotubes (b,c).

In all the investigated SWNTs ropes (more than 20), EELS signals of boron and nitrogen were simultaneously and locally detected. A representative example of this key feature is analyzed in detail in Figure 2. Figure 2a represents the bright field image of a nanotubes rope of 4−5 nm in width, which is assumed to consist of less than eight nanotubes, referring to HRTEM images of bundles displaying a similar width. A spectrum image has been acquired over a 98×24 nm^2 region of the rope marked in Figure 2a. For each of the 1024 probe positions, both the whole EELS spectrum encompassing the K edges for boron, carbon, and nitrogen and the high angle annular dark field signal were recorded in parallel with an acquisition time of 200 ms. A first indication about the distribution of B, N, and C atoms within the rope is obtained from the three element intensity maps extracted from the spectra and displayed in Figure 2b. Let us consider the areas marked, area I and area II, respectively, along the rope. Their surface is 20×3 nm^2 and corresponds to an ensemble of 30 spectra. In area I, a signal is clearly simultaneously detected for both B and N. In area II, on the contrary, neither B nor N is detected. We note that the mapping for nitrogen is rather noisier than that for boron and carbon in Figures 2c and 4c, respectively, due to the weaker N 1s ionization cross section. This first indication that B and N are not homogeneously distributed along the rope but self-assembled into small domains is confirmed by considering in Figure 2c the sums of the spectra recorded in area I and area II and spectrum I and spectrum II, respectively. The three characteristic K edges for B, C, and N are clearly visible in spectrum I at 188, 284, and 401 eV, respectively, while B and N signals are absent from spectrum II. Thanks to the definition of the areas I and II, the spectra

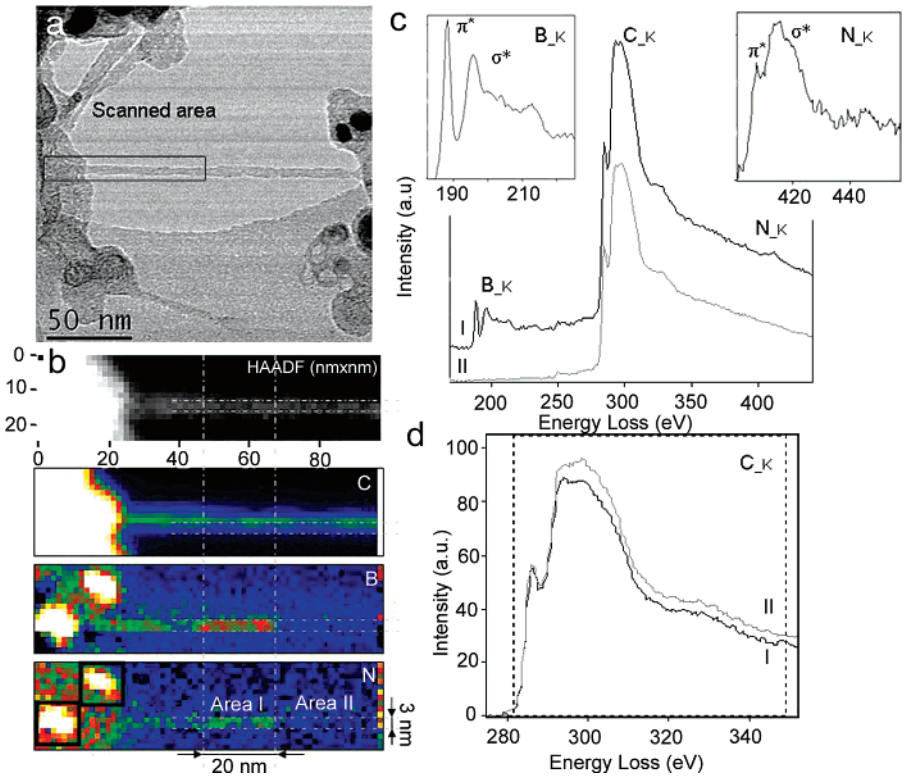

Figure 2. (a) Bright-field image of nanotubes rope of 4−5 nm large. The rectangle shows the region analyzed by EELS and corresponds to a 64 × 16 pixels spectrum image. (b) HADF image of the scanned area of 98 × 24 nm^2 and the relative intensity chemical maps of C, B, and N elements. The intensity of the signal varies from dark/blue (poor signal) to white/red (high signal) colors. Areas marked area I and area II have a surface of 20 × 3 nm^2 and are defined at the positions 50−70 nm and 70−90 nm along the tube axis, respectively. (c) EEL spectra I and II are defined as the sum of the sum of areas I and II, respectively. Each spectrum is the sum of 30 spectra. Near edge-fine structures of B and N−K edges are shown in the inset. (d) Background subtracted C−K edges of the I and II areas.

are quantitatively comparable so that the change in the C, B, and N concentrations between areas I and II can be determined from the intensities of the K edges of spectra I and II. The concentration in carbon is found to decrease by 10 atom % from area II to area I, whereas the concentration of B and N is estimated to lie between 4 and 10 atom % in area I. No variation in the carbon K edge is detected when analyzing in the same way a volume of the rope equivalent to areas I + II located just above and which does not display any B or N signals. These analyses lead to the conclusion that, in area I, part of the carbon atoms (about 10 atom %) has been replaced by B and N, forming a nanodomain embedded in the carbon network.

Close inspections of the near-edge fine structures (ELNES) provide information on the structure of this nanodomain and its junction with the carbon network. First, whatever the area considered, C−K ELNES (Figure 2d) are very similar to those observed usually on pure carbon SWNTs ropes[38] and display the usual π^* and σ^* features characteristic of the sp^2 bonding. Second, structure of BN domains can be investigated by analyzing the fine structure of B−K and N−K edges, which are ideal fingerprints thanks to their high sensitivity to variations in chemical and structural environment.[39,40] For example, as shown in Figure 3a, B−K ELNES recorded in h-BN, B_2O_3, B_4C, and pure B reference samples display significant differences, allowing one to clearly discriminate between the different chemical environments of boron in these samples. One can also consider the B−K ELNES in CB_x MWNTs studied by Vieira et al.[41] Figure 3b displays for comparison B−K ELNES recorded on different BN nanostructures, from top to bottom, pure BN SWNTs,[35,40] BN nanodomains of our C−BN ropes (area I of Figure 2b) and an amorphous BN area present in the same sample (square marked in Figure 2b). Similarly, the N−K ELNES recorded on pure BN SWNTs, BN nanodomains of our C−BN ropes, and N-substituted SWCNTs[42] are shown from top to bottom on Figure 3c.

A key point is the striking similarity between the B−K and N−K fine structures of the nanodomains and of that of BN SWNTs and h-BN. All of these spectra display a 1s → π^* transition peak and a series of 1s → σ^* transition peaks characteristic of the sp^2 B−N bonding. However, some discrepancies are noticeable that appear to be larger for N−K than for the B−K edge. Let us discuss first the B−K edge. The π^*/σ^* ratio intensity varies depending on the probe position along the C−B−N rope. This variation could be due to anisotropic effects related to a random distribution of the BN nanodomains all around the circumference of the nanotube. Indeed, as shown in Figure 3a, B−K edge in h-BN is orientation dependent and the π^*/σ^* ratio intensity is strongly varying whether the hexagonal layer is parallel or perpendicular to the electron beam (momentum perpendicular or parallel respectively).[40,43,44] This anisotropic effect is strongly attenuated in the BN SWNTs signal because, due to the nanometer size of the probe, it is averaged on all the orientations of a BN layer. The second difference between

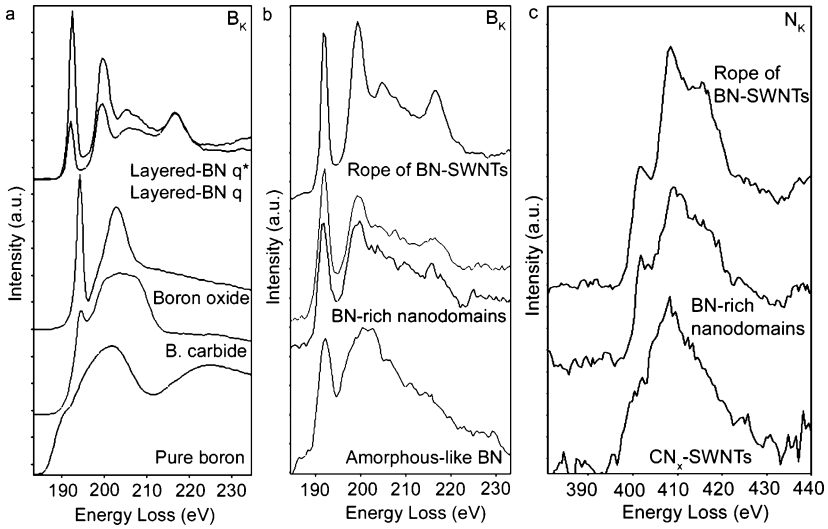

Figure 3. (a) ELNES B−K edges of different boron chemical states taken as references. q* and q are, respectively, the perpendicular and parallel momentum transfer vectors to the *c*-axis of the h−BN layers. (b) and (c) ELNES B−K and N−K edges from experimental analysis on BN SWNTs, CN_x SWNTs from previous studies,[40,42] and from the C−BN SWNTs sample.

B−K ELNES of BN SWNTs and BN domains of C−B−N SWNTs lies in the intensity sharpness of the σ^* peak, which is less definite for BN nanodomains than for pure BN SWNTs and in the structuration of the σ^*, which is also partially lost. These discrepancies are subtle, and this loss of structuration could mainly be a consequence of the finite size fo the BN domains. In any case, these perturbations of the fine structure seem not to reflect the presence of C−B bonds, which would give rise to a low-energy shift of the π^* peak and to a drastic difference of the σ^* band.[41]

The loss of structuration is much more pronounced for the N−K σ^* band (Figure 2c), which shows an intermediate behavior between that of BN SWNTs and that of CN_x MWNTs. We suggest that all the reported differences could be the signature of subtle changes in the electronic structure resulting mainly from the finite size of the BN domains and from the contribution of the C−B and C−N bonds at the BN nanodomains/C interface. The fact that N−K ELNES is more perturbed than B−K ELNES suggests a more important contribution of C−N bonds than that of C−B bonds and could indicate that boundaries between BN domains and the C network dominantly involve C−N bonds. This preferential tendency is consistent with the higher ability of nitrogen to be incorporated in carbon nanotubes because, as found experimentally, concentrations in nitrogen exceeding 10 atom % can be achieved,[45,46] whereas concentrations in boron, in all experimental synthesis attempts, remains very low.[47,48,41] To go further, ab initio calculations would be needed on C−BN heterostructures to study in detail the local density of unoccupied states as probed by EELS. Finally, B−K ELNES of BN nanodomains can clearly be distinguished from that of amorphous areas shown in Figure 3b. In this latter nanostructure, the intensity of the peak for boron K edge is strongly reduced and the structuration of the band is partially lost. Such fine structures have never been detected in the ropes, then excluding any contamination of the SWNTs by an amorphous structure. As well, the presence of small carbide clusters on or within the ropes can also be excluded.

To summarize, it can be deduced from this detailed ELNES analysis that, when present along a SWNT, B and N are in substitution of C and replace C at the vertices of the hexagonal network in order to build a piece of an hexagonal BN layer forming preferentially C−N bonds at the interface with the C lattice. Let us discuss now the shape and size of this BN piece, referring to the example analyzed in Figures 2 and 3. The dimension of area I in Figure 2 is about 3 nm large and 20 nm long. We know from the determination of the relative concentrations of C, B, and N in the areas where B and N are present, that only 10 atom % of carbon atoms of the rope are substituted by B and N. Owing to the reduced number of nanotubes present in this rope (about eight tubes), the number of projected nanotubes analyzed through the electron beam, when the beam is scanned over area I, should not exceed one or two. If we assume that C is substituted for only one of these two nanotubes, the substitution concerns 40 atom % of C atoms in an area of 60 nm^2. According to semiempirical calculations on the stability of C−BN-like segregated patterns, only two configurations are found to be stable.[7] In the first configuration, the BN domain is a strip wrapped around the nanotube, whereas in the second one, it is an island embedded in the carbon network. Applying these results to the example of Figure 2, the BN nanodomains would be either a strip made of two adjacent zigzag chains of 1 nm long or an island made of three adjacent hexagons per nm^2 (1 $nm^2 \approx 18$ hexagons ($\times 2$)). Note that this value is an average value per nm^2. Considering the pixel size in our experiment (between 1.5 nm × 1.5−2 nm × 2 nm), patches of 12 hexagons per 4 nm^2, which would correspond to a higher segregation of BN bonds, are possible. Note also that, occasionally, a higher concentration in BN has also been observed and can reach 25−30 atom % in a nanotube rope, but such situations are not representative of the average structure of the SWNTs. The BN domains have the very important property of being present at several places along a given rope. A typical example is given in Figure 4. The analyzed area corresponds to a rope of 50 nm long and 12

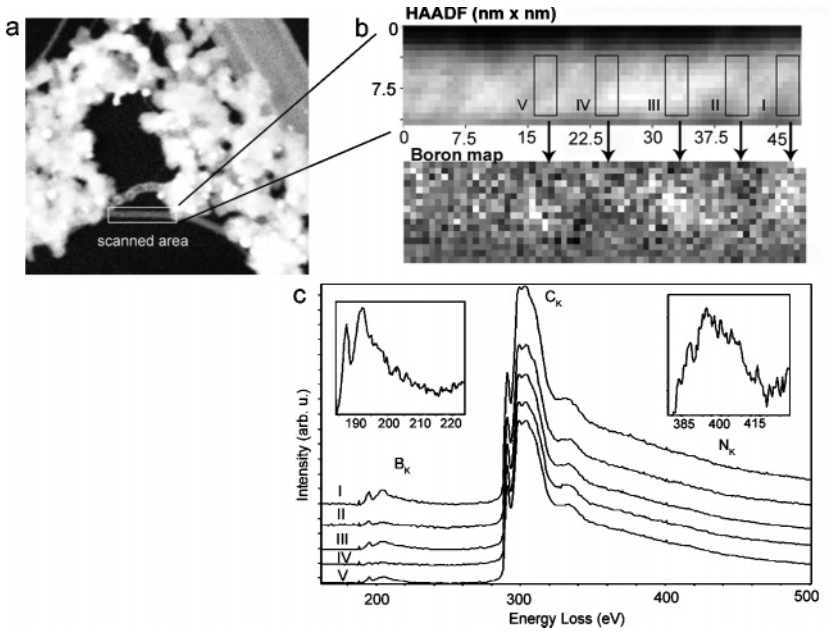

Figure 4. (a) HADF image of a nanotubes rope. The rectangle shows the region analyzed by EELS. (b) 64 × 16 Pixel spectrum image of a 50 × 12 nm^2 area of the nanotubes rope acquired with an acquisition time of 300 ms and the boron chemical map. (c) EEL spectra associated with the I, II, III, IV, and V marked areas. Each spectrum is the sum of respectively 44 spectra and corresponds to 3 × 9 nm^2 areas in the nanotubes rope. Concentration of B and N in I, III, and V do not exceed 4 atom % locally.

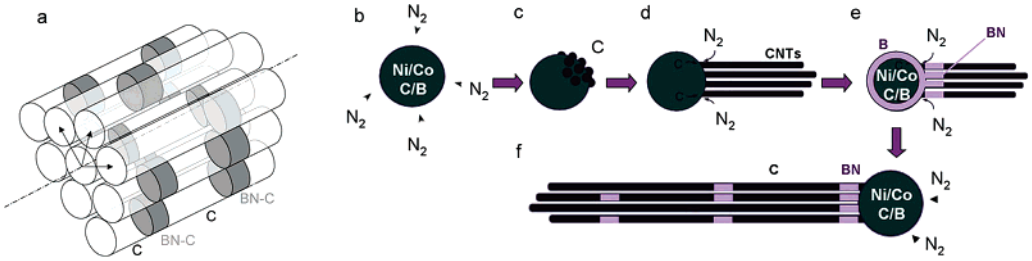

Figure 5. (a) Sketch of the structure of a bundle made of C−BN SWNTs. (b−f) Scenario derived from the V−L−S model.[49] (b) Formation of metal liquid nanoparticle saturated with carbon and boron. (c) Carbon segregation and nucleation of nanotubes. (d) Growth of nanotubes until (e) boron appears at the surface of the nanoparticles and reacts with the nitrogen gas to form BN nanodomains. (f) Sequential growth with a longitudinal segregation of BN nanodomains C−BN−(C−BN)n-like.

nm large. Each EEL spectrum associated to the I, II, III, IV, and V marked areas are the sum of 44 spectra of a region of 3 × 9 nm^2. Both B and N are present in spectra I, III, and V, and a relative quantification of the signal showed that these atoms have replaced only a weak fraction of C atoms. This sequential behavior concerns several nanotubes within the same rope, and the substitution phenomenon is limited to smaller areas than in the rope described in Figure 2. We estimate the B and N concentrations to be less than 3−4 atom % locally and less than 2 atom % in average, knowing that the detection limit for boron is 0.1−0.2 atom %.

The results presented above support the structure of the ropes sketched in Figure 5a where the nanotubes exhibit C−BN-rich nanodomains in substitution of C on the atomic sites of the honeycomb network. We have therefore to account for the formation of these domains and explain why the C−BN segregation is sequential along the axis of SWNTs. The model we propose here refers to the phenomenological models put forward to account for the formation of both C SWNTs[49] and BN SWNTs[35,40] grown using the laser vaporization technique. For clarity, these models are briefly recalled first. In the first case, the model is based on a V−L−S model. Carbon issued from the vaporization of the target condenses first in the form of small aggregates. When the temperature falls below 2000 K, metal vapor then condenses as liquid nanodroplets, which can solubilize the primarily formed carbon aggregates. Upon cooling, the metal particles get supersaturated in carbon, leading to its segregation. Because of its low surface tension (one order scale lower than liquid Ni or Co) and the small size of the particle, carbon diffuses toward the surface of the particle and precipitates in the form of small graphitic caps, which are SWNTs nuclei. This nucleation mechanism implies a root growth mechanism where carbon is progressively incorporated at the foot of the nanotube via its interface with the particle surface, where the bonds are the most reactive. The formation of BN SWNTs proceeds in a different manner because, in that case, no metal catalyst is required. The h-BN compound of the target does not sublimate as graphite does, but decomposes above 2600 K into gaseous nitrogen and in liquid boron, which gets vaporized. Upon cooling, the boron vapor then condenses into small liquid droplets, and the formation of

the BN SWNTs results from the reaction of the highly reactive boron droplets with nitrogen gas. As in the previous case, the growth is a root-based mechanism. Moreover, the particularity of the continuous CO_2 laser is that the carrier gas of the reactor is heated in the vicinity of the target and acts as a local furnace, leading to a stationary regime where the SWNT growth kinetics is compatible with the cooling kinetics of the nanoparticles.[49] On the basis of these two models, we propose a scenario presented in the Figure 5.

As for C SWNTs, the process involves the formation of liquid nanoparticles of Ni/Co catalysts (Figure 5b). But now, both carbon and boron can be solubilized in these particles. In particular, according to the M (M = Ni, Co)-B phase diagrams, boron is highly soluble in Ni and Co liquids at high temperature.[50] Therefore, in spite of its low fraction in the target, boron will preferably be incorporated in the metal particle rather than condense into boron droplets. Upon cooling, particles get supersaturated in carbon and in boron. For both elements, segregation proceeds via their diffusion toward the surface of the particles owing to their surface tension to be below that of liquid Ni and Co (C: 150 mJ/m^2 at 1500 °C; B: 1060 mJ/m^2 at 2077 °C, liquid Ni and Co: 1500 mJ/m^2 at 1500 °C[50,51]).[52] Carbon is assumed to segregate first. The first reason lies in its higher concentration in the system and its lower solubility limit in Co and Ni. The second argument lies in the properties of the B−C−N equilibrium phase diagram, which indicates, that, when the concentration of the system is carbon rich and under a sufficient nitrogen pressure, the first solid phase occurring upon cooling is graphite.[11,12] This is a direct consequence of the fact that the compositions considered here are on the carbon-rich side of the eutectic point of the C−BN phase diagram. Once expulsed, carbon crystallizes at the surface of the particle, leading to the formation of single-walled nanotubes nuclei as for pure C-SWNTs (Figure 5c).

The growth proceeds through further incorporation of carbon at the root of the nanotubes (Figure 5d) unless boron comes at the nanoparticle surface (Figure 5e). This boron segregation process is attested by the observation, in the sample, of boron precipitates partially covering the surface of some Ni/Co particles as in the example shown in Figure 6.

Once at the surface, boron is highly reactive. Because the B−N bond is much more stable than the B−C bond, boron reacts immediately with nitrogen gas instead of being incorporated in the C network. This reaction leads to the incorporation of nitrogen in the active sites at the root of the growing C SWNTs and to the formation of a honeycomb BN network instead of the carbon one (Figure 5f). The perfect agreement between the lattice parameters of both networks certainly facilitates the substitution. Once the boron present at the surface is consumed, SWNT growth continues with carbon atoms incoming at its foot. BN nanodomains will form each time some boron atoms are present at the surface of the particle, explaining the sequential presence of BN nanodomains along a given rope. The arguments put forward to account for the formation of separate BN and C domains are based on energetic considerations and on the

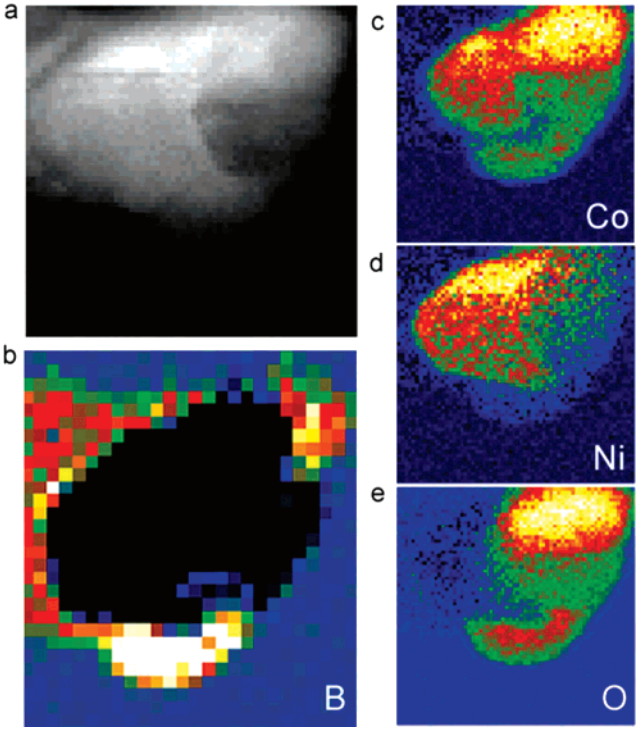

Figure 6. 64 × 64 Spectrum image corresponding to a 50 × 50 nm^2 area over a nanoparticle acquired with an acquisition time of 300 ms. (b,c,d,e) are respectively the chemical maps of boron, cobalt, nickel, and oxygen. Boron is present as an oxide at the nanoparticle surface due to its oxidation with air at the end of the synthesis.

phase separation between graphite and h-BN. The sequence of BN domains along a given rope mimics the two-phase patterns, found in unidirectional eutectic growth with a separation into domains of each phase at the solidification front of a liquid phase. The theoretical C−BN phase diagram gives striking evidence for such an eutectic solidification of a liquid + gas phase into graphite and a BN-rich phase.[11] This property of the phase diagram has already been put forward to account for the sandwich structure found in C−BN−C MWNTs synthesized using the electric arc discharge.[20] In that case, due to the formation of concentric multiple tubular layers, the phase patterning induced by the eutectic transformation was 2D. Here the formation of a single-walled nanotube implies the development of the patterning along the tube axis. BN domains remain very small probably because of the large excess of C compared to B, which prevents the formation of pure BN SWNT.

We have shown that it is possible to directly synthesize, using a continuous CO_2 laser vaporization reactor, single-walled carbon nanotubes that contain BN nanodomains embedded in the carbon network in a sequential manner along the tube axis. HRTEM analyses coupled with electron energy loss spectroscopy in a STEM with a subnanometer probe provide direct evidence of the patterning of the honeycomb lattice by BN and C domains. The BN entities are a few nanometers square and replace not more than 10 atom % of C locally and 5 atom % on average within a given rope. The formation of these patterned tubes is analyzed to be a direct consequence of the segregation phase existing at

equilibrium between graphite and h-BN. The observations support a growth mediated by a liquidlike phase as in the V−L−S model invoked in the formation of C SWNTs. The sequence of BN domains alternating with long C segments along the tube axis is the result of a phase separation at the solidification front. The structure of the present C−BN tubes therefore appears to be governed by thermodynamical properties of the C−B−N system, although its formation is due to particular kinetic conditions. One can in turn consider using these properties to adjust the synthesis conditions in order to produce SWNTs with anticipated BN−C patterning and obtain different electronic devices.

Acknowledgment. This work was supported by the Office National d'Etudes et de Recherche Aérospatiale (ONERA) and Arkema Group, France. This work has been done in the framework of the GDRE n 2756 "Science and applications of nanotubes"—NANO-E.

References

(1) Hamada, N.; Sawada, S.; Oshiyama, A. *Phys. Rev. Lett.* **1992**, *68*, 1579.
(2) Blase, X.; Rubio, A.; Louie, S. G.; Cohen, M. L. *Europhys. Lett.* **1994**, *28*, 335.
(3) Arenal, R.; Stéphan, O.; Kociak, M.**;** Taverna, D.; Loiseau; A.; Colliex, C. *Phys. Rev. Lett.* **2005**, *95*, 127601.
(4) Lauret, J. S.; Arenal, R.; Ducastelle, F.; Loiseau, A.; Cau, M.; Attal-Trétout, B.; Rosencher, E.; Goux-Capes, L. *Phys. Rev. Lett.* **2005**, *94*, 037405.
(5) Wirtz, L.; Marini, A.; Rubio, A. *Phys. Rev. Lett.* **2006**, *96*, 126104.
(6) Park, C. H.; Spataru, C. D.; Louie, S. G. *Phys. Rev. Lett.* **2006**, *96*, 126105.
(7) Nozaki, H.; Itoh, S. *J. Phys. Chem. Solids* **1996**, *57*, 41.
(8) Blase, X., Charlier, J.-Ch.; De Vita, A.; Car, R. *Appl. Phys. A* **1999**, *68*, 293.
(9) Mazzoni, M. S. C.; Nunes, R. W.; Azevedo, S.; Chacham, H. *Phys. Rev. B* **2006**, *73*, 073108.
(10) Liu, A. M.; Wentzcovitch, R. M.; Cohen, M. L. *Phys. Rev. B.* **1989**, *39*, 1760.
(11) Kasper, B. Ph.D. Thesis. Ph.D. Thesis, Stuttgart University, 1996.
(12) Seifert, H. J.; Lukas, H. L.; Aldinger, F. *Ber. Bunsen-Ges. Phys. Chem.* **1998**, *102*, 1309.
(13) Blase, X.; Charlier, J.-Ch.; De Vita, A.; Car, R. *Appl. Phys. Lett.* **1997**, *70*, 197.
(14) Kaner, R. B.; Kouvetakis, J.; Warble, C. E.; Sattler, M. L.; Bartlett, N. *Mater. Res. Bull.* **1987**, *22*, 399.
(15) Watanabe, M. O.; Itoh, S.; Sasaki, T.; Mizushima, K. *Phys. Rev. Lett.* **1996**, *77*, 187.
(16) Chen, Y.; Barnard, J. C.; Palmer, R. E.; Watanabe, M. O.; Sasaki, T. *Phys. Rev. Lett.* **1999**, *83*, 2406.
(17) Stéphan, O.; Ajayan, P. M.; Colliex, C.; Redlich, P.; Lambert, J. M.; Bernier, P.; Lefin, P. *Science* **1994**, *266*, 1683.
(18) Redlich, Ph.; Loeffler, J.; Ajayan, P. M.; Bill, J.; Aldinger, F.; Rühle, M. *Chem. Phys. Lett.* **1996**, *260*, 465.
(19) Zhang, Y.; Gu, H.; Suenaga, K.; Iijima, S. *Chem. Phys. Lett.* **1997**, *279*, 264.
(20) Suenaga, K.; Willaime, F.; Loiseau, A.; Colliex, C. *Appl. Phys. A* **1999**, *68*, 301.
(21) Kohler-Redlich, Ph.; Terrones, M.; Manteca-Diego, C.; Hsu, W. K.; Terrones, H.; Rühle, M.; Kroto, H. W.; Walton, D. R. M. *Chem. Phys. Lett.* **1999**, *310*, 459.
(22) Ma, R.; Bando, Y.; Sato, T. *Chem. Phys. Lett.* **2001**, *350*, 1.
(23) Ma, R.; Bando, Y. *Adv. Mater.* **2003**, *4*, 403.
(24) Golberg, D.; Dorozhkin, P. S.; Bando, Y.; Dong, Z.-C.; Grobert, N.; Reyes-Reyes, M.; Terrones, H.; Terrones, M. *Appl. Phys. Lett.* **2003**, *82*, 1275.
(25) Suenaga, K.; Colliex, C.; Demoncy, N.; Loiseau, A.; Pascard, H.; Willaime, F. *Science* **1997**, *278*, 653.
(26) Golberg, D.; Dorozhkin, P. S.; Bando, Y.; Mitome, M.; Tang, C. C. *Diamond Rel. Mater.* **2005**, *14*, 1857.
(27) Han, W. Q.; Cumings, J.; Zettl, A. *Appl. Phys. Lett.* **2001**, *78*, 2769.
(28) Han, W. Q.; Cumings, J.; Huang, X.; Bradley, K.; Zettl, A. *Chem. Phys. Lett.* **2001**, *346*, 368.
(29) Golberg, D.; Dorozhkin, P.; Bando, Y.; Hasegawa, M.; Dong, Z.-C. *Chem. Phys. Lett.* **2002**, *359*, 220.
(30) Wang, R. M.; Zhang, H. Z. *New J. Phys.* **2004**, *6*, 1.
(31) Terrones, M.; Golberg, D.; Grobert, N.; Seeger, T.; Reyes-Reyes, M.; Mayne, M.; Kamalakaram, R.; Dorozhkin, P.; Dong, Z. C.; Terrones, H.; Rühle, M.; Bando, Y. *Adv. Mater.* **2003**, *15*, 1899.
(32) Zhi, C. Y.; Guo, D.; Bai, X. D.; Wang, E. G. *J. Appl. Phys.* **2002**, *91*, 5325.
(33) Wang, W. L.; Bai, X. D.; Liu, K. H.; Xu, Z.; Golberg, D.; Bando, Y.; Wang, E. G. *J. Am. Chem. Soc.* **2006**, *128*, 6530.
(34) Cochon, J.-L.; Gavillet, J.; Lamy de la Chapelle, M.; Loiseau, A.; Ory, M.; Pigache, D. *AIP Conf. Proc.* **1999**, *486*, 237.
(35) Lee, R. S.; Gavillet, J.; Lamy de la Chapelle, M.; Loiseau, A.; Cochon, J.-L.; Pigache, D.; Thibault, J.; Willaime, F. *Phys. Rev. B* **2001**, *64*, 121405.
(36) Jeanguillaume, C.; Colliex, C. *Ultramicroscopy* **1989**, *28*, 252.
(37) Colliex, C.; Tencé, M.; Lefèvre, M.; Mory, C.; Gu, H.; Bouchet, D.; Jeanguillaume, C. *Mikrochim. Acta* **1994**, *71*, 114.
(38) Suenaga, K.; Sandre, E.; Colliex, C.; Pickard, C. J.; Kataura, H.; Iijima, S. *Phys. Rev. B* **2001**, *63*, 165408.
(39) Stéphan, O.; Vlandas, A.; Arenal, R.; Loiseau, A.; Trasobares, S.; Colliex, C. In *Proceedings of EMAG Conference*; Institute of Physics: Bristol, U.K., 2003.
(40) Arenal, R. Ph.D. Thesis, Université de Paris XI, Orsay, 2004.
(41) Vieira, S. M. C.; Stéphan, O.; Carroll, D. L. *J. Mater. Res.* **2006**, *21*, 3058.
(42) Enouz-Védrenne, S. Ph.D. Thesis, Université de Montpellier 2, 2007.
(43) Stéphan, O.; Sandré, E.; Ajayan, P. M.; Cyrot-Lackman, F.; Colliex, C. *Phys. Rev. B.* **1996**, *53*, 13824.
(44) Souche, C.; Jouffrey, B.; Hug, G.; Nelhiebel, M. *Micron* **1998**, *29*, 419.
(45) Glerup, M.; Castignolles, M.; Holzinger, M.; Hug, G.; Loiseau, A.; Bernier, P. *Chem. Commun.* **2003**, *20*, 2542.
(46) Tang, C.; Bando, Y.; Golberg, D.; Xu, F. *Carbon* **2004**, *42*, 2625.
(47) Blase, X.; Charlier, J.-Ch.; De Vita, A.; Car, R.; Redlich, P.; Terrones, M.; Hsu, W. K.; Terrones, H.; Caroll, D. L.; Ajayan, P. M. *Phys. Rev. Lett.* **1999**, *83*, 5078.
(48) Gai, P. L.; Stéphan, O.; McGuire, K.; Rao, A. M.; Dresselhaus, M. S.; Dresselhaus, G.; Colliex, C. *J. Mater. Chem.* **2004**, *14*, 669.
(49) Gavillet, J.; Loiseau, A.; Journet, C.; Willaime, F.; Ducastelle, F.; Charlier, J.-Ch. *Phys. Rev. Lett.* **2001**, *87*, 275504.
(50) Okamoto, H. *Phase Diagram for Binary Alloys: Handbook*; ASM International: Materials Park, OH, 2000.
(51) Eustathopoulos, N.; Nicholas, M. G.; Drevet, B. Wettability at High Temperatures. Pergamon Materials Science: Elmsford, NY, 1999.
(52) Moreover, the equilibrium vapour pressure over a spherical particle increases with increasing curvature of the particle (Kelvin effect), emphasizing the formation of aggregates at the metal surface.

NL070327Z